PHYSICAL REVIEW B **92**, 205310 (2015)

Two-dimensional oxide topological insulator with iron-pnictide superconductor LiFeAs structure

Qiunan Xu,[1] Zhida Song,[1] Simin Nie,[1] Hongming Weng,[1,2,*] Zhong Fang,[1,2] and Xi Dai[1,2]

[1]*Beijing National Laboratory for Condensed Matter Physics, and Institute of Physics, Chinese Academy of Sciences, Beijing 100190, China*

[2]*Collaborative Innovation Center of Quantum Matter, Beijing, China*

(Received 15 September 2015; revised manuscript received 5 November 2015; published 24 November 2015)

By using first-principles calculations, we propose that ZrSiO can be looked at as a three-dimensional (3D) oxide weak topological insulator (TI) and its single layer is a long-sought-after 2D oxide TI with a band gap up to 30 meV. Calculated phonon spectrum of the single layer ZrSiO indicates it is dynamically stable and the experimental achievements in growing oxides with atomic precision ensure that it can be readily synthesized. This will lead to novel devices based on TIs, the so-called "topotronic" devices, operating under room temperature and stable when exposed in the air. Thus a new field of "topotronics" will arise. Another intriguing thing is this oxide 2D TI has the similar crystal structure as the well-known iron-pnictide superconductor LiFeAs. This brings great promise in realizing the combination of superconductor and TI, paving the way to various extraordinary quantum phenomena, such as topological superconductor and Majorana modes. We further find that there are many other isostructural compounds hosting the similar electronic structure and forming a WHM family with W being Zr, Hf, or La, H being group IV or group V element, and M being group VI one.

DOI: 10.1103/PhysRevB.92.205310 PACS number(s): 73.22.−f, 73.43.−f, 71.70.Ej, 85.75.−d

I. INTRODUCTION

Topological insulator (TI) has nontrivial band topology characterized by Z_2 topological invariant under time-reversal symmetry (TRS) [1–3]. Similar to the systems with integer quantum Hall effect, the bulk band structure of TIs is insulating with unavoidable edge or surface states on the boundary connecting the valence and conduction bands. Especially for the two-dimensional (2D) TI, it can host quantum spin Hall effect (QSHE) with 1D helical edge states, where the states moving in opposite direction have opposite spin. Therefore, the backscattering is prohibited as long as the scattering potential does not break TRS and such helical edge states provide a new mechanism to realize nondissipative electronic transportation, which promises potential application in a low-power and multifunctional device based on TI. From this point of view, a 2D TI with large band gap, chemically stable under ambient condition exposed in the air, easy to prepare and consisting of cheap and nontoxic elements is highly desired [4,5]. The study of TI based quantum devices would foster a field of "topotronics". Such 2D TI is also important and crucial to the realization of topological superconductivity and Majorana modes through proximity effect [2,6].

However, up to now there are only a few systems which have been proved to be 2D TI [5,7], such as the quantum well of HgTe/CdTe [8,9] and InAs/GaSb [10]. Both of the above systems require very sophisticated and expensive MBE growth and only show QSHE at ultralow temperature. These extreme requirements have obstructed further studies and possible applications of 2D TIs. The theoretical efforts in finding and designing 2D TI candidates keep going on and some of them are listed here: silicene [11], chemically decorated single layer honeycomb lattice of Sn [12], Ge [13], and Bi or Sb [14–16], buckled BiF [17], single layer $ZrTe_5$, $HfTe_5$ [18], and Bi_4Br_4 [19], transition-metal dichalcogenide (TMD) in 1T′ [20], and haeckelite [21–24] structure. But none of them has been confirmed experimentally. Recently, Weng *et al.* proposed a large band gap 2D TI in oxygen functionalized MXene [4], which brings the hope in realizing TI in oxygen contained compounds, which are naturally antioxidant and stable when exposed in the air. This also stimulated the effort in this paper in searching for new oxide TIs.

In this paper, by using first-principles calculations we demonstrate that the oxide material ZrSiO is a weak TI and a single layer of it is a 2D TI with achievable band gap up to 30 meV [25–27]. We have calculated its edge states and analyzed the physical mechanism for band inversion. We have found many other isostructural compounds with formula of WHM (W = Zr, Hf, or La, H = Si, Ge, Sn, or Sb, and M = O, S, Se, and Te) possessing the similar electronic structure.

II. COMPUTATIONAL DETAILS

We have employed the Vienna *ab initio* simulation package (VASP) [28,29] for most of the density functional theory (DFT) based first-principles calculations. Exchange-correlation potential is treated within the generalized gradient approximation (GGA) of Perdew-Burke-Ernzerhof type [30]. Spin-orbit coupling (SOC) is taken into account self-consistently. The cutoff energy for plane wave expansion is 500 eV and the k-point sampling grid in the self-consistent process was $12 \times 12 \times 3$ for the 3D case and $12 \times 12 \times 1$ for the single layered structure. The crystal structures have been fully relaxed until the residual forces on each atom are less than 0.001 eV/Å. A vacuum around 16 Å between layers was used to minimize the interactions between the layer and its periodic images. The possible underestimation of band gap within GGA is checked by the nonlocal Heyd-Scuseria-Ernzerhof (HSE06) hybrid functional [31,32] calculation. To explore the edge states, we build a tight-binding model for a slab around 120 unit cell thick with edges along the a or b lattice [3,5]. The maximally localized Wannier functions (MLWF) [33,34] of d orbitals of W and p orbitals of H are generated as the basis set by using the software package OPENMX [35,36].

*hmweng@iphy.ac.cn

 ©2015 American Physical Society

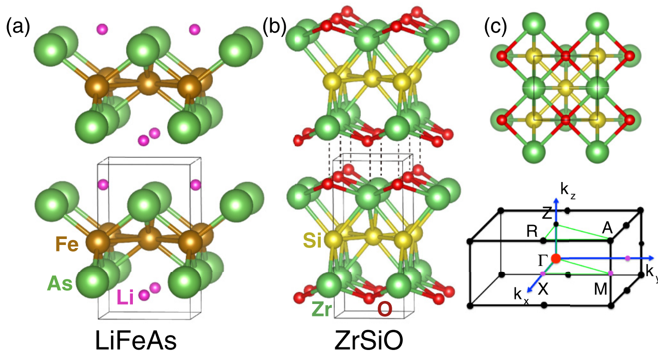

FIG. 1. (Color online) Crystal structure of (a) LiFeAs and (b) ZrSiO. (c) Top view of single layer ZrSiO and 3D Brillouin zone with high symmetrical crystal momenta indicated. The weak bonds between Si-O have been indicated by dashed lines, which form a natural cleavage plane to get 2D single layer ZrSiO.

III. RESULTS AND DISCUSSION

Crystal structure. The bulk ZrSiO belongs to a big family of ZrSiS- (or PbFCl-) type compounds [37] with chemical formula of WHM (W=transition metal or rare earth element; H, M=main group elements). There are over 200 members in this family [38], and the crystal structure in Fig. 1 can be looked at as stacking of five square nets of W, H, and M in the sequence of [$\ldots M$-W-H-W-$M\ldots$] along c axis. The relatively weak M-W bonding connecting two neighboring slabs shown in Fig. 1 leads to a quasilayered structure of them. In fact, it was thought that the crossover from 3D to 2D in ZrSiM (M = O, S, Se, and Te) happens between M = Se and Te [39]. Nevertheless, this gives out a natural cleavage plane for getting a 2D layer of these compounds and we will show the band dispersion along c is quite narrower than that of in-plane for several members in this family. It is noticed that the isostructural pnictide NbSiAs has been found to be superconductor [40]. The intensively studied iron-pnictide superconductor LiFeAs also has the isostructure but with the cation and anion sites being switched to form the so-called anti-PbFCl (or anti-ZrSiS) type structure [41]. The space group of ZrSiO is $P4/nmm$ (no. 129). The theoretically optimized lattice constants are $a = b = 3.316$ Å and $c = 7.354$ Å, being underestimated by about 6%–7% compared with experimental values $a = b = 3.52$ Å and $c = 7.93$ Å [37]. This is within the common error in lattice constant estimation from DFT calculation within GGA. The optimized Wyckoff site of atoms are Zr (0.25, 0.25, 0.308), Si (0.75, 0.25, 0), and O (0.25, 0.25, 0.6112), also consistent with the experimental values. The general features of the band structure from the optimized crystal structure and the experimental one are quite similar. To be consistent in the description of the main text, the theoretically optimized crystal structure is used in the following discussion.

Band structure of 3D ZrSiO. The band structure of 3D ZrSiO is shown in Fig. 2(a). There are two distinct features. One is the apparent band crossing points around the Fermi level indicating the existence of band inversion as found in many other materials [18,21] with nontrivial topological band structures [3,5]. The second feature is its band dispersion in $k_z = 0$ plane (Γ-X-M-Γ) resembles that in $k_z = \pi$ plane (Z-R-A-Z) and there is no band inversion happen along Γ-Z direction. This means that its electronic structure is essentially more 2D like than 3D. The further group theory analysis indicates that the bands crossing in both $k_z = \pi$ and 0 planes are protected by glide mirror perpendicular to the z axis because the two bands forming the crossing points belong to different eigenvalues of that glide mirror. As discussed in Refs. [42–45], these band crossing points form a closed node-line circle in the $k_z = 0$ and $k_z = \pi$ plane, respectively, when

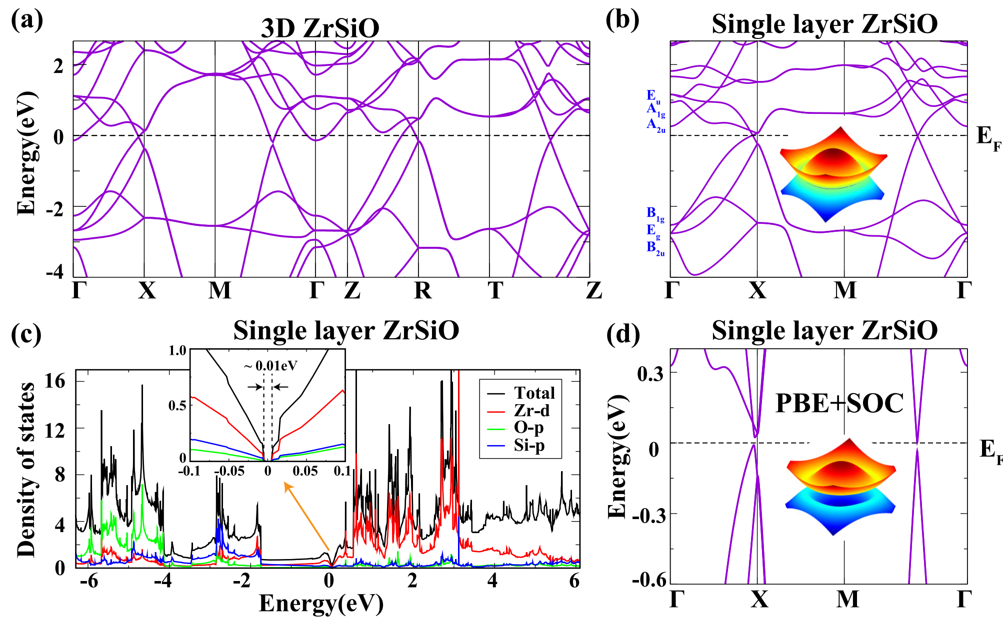

FIG. 2. (Color online) Band structure for (a) bulk ZrSiO within GGA and single layer ZrSiO within (b) GGA and (d) GGA+SOC. (c) is the total DOS of single layer ZrSiO. The inset in (b) indicates the node-line due to band inversion around Fermi level protected by in-plane mirror symmetry. The inset in (d) indicates the gap opening in node line when SOC is further included.

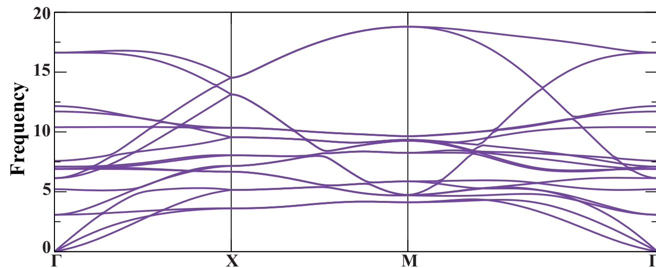

FIG. 3. (Color online) Phonon spectrum of optimized single layer ZrSiO.

SOC is not considered. Including SOC into the calculation opens a gap along the node lines turning 3D ZrSiO into a system with finite gap at all k points but compensated electron and hole pockets at the Fermi level. As we have discussed in Refs. [43,44], the crossing points on the node line are not exactly on the same energy level due to the particle-hole asymmetry. There will be a finite global band gap instead of compensated electron-hole pockets. Since the material has an inversion center, we can determine its Z_2 invariances through the production of the parities at the time reversal invariant momenta (TRIM), which gives (0; 001) indicating that it is a weak TI if the band gap opening on the node lines due to SOC is large enough to open the indirect gap [25,26]. The above results also indicate that 3D ZrSiO can be viewed as the stacking of 2D TI along the c axis [25,26], similar to $ZrTe_5$ [18] and Bi_4Br_4 [19].

2D TI of single layer ZrSiO. As discussed above, we take a single layer of ZrSiO by breaking the weak Si-O bonds. In order to get the binding energy between layers of ZrSiO, we calculate the total energies of 3D and single layer ZrSiO with the same setting of parameters in calculations. The binding energy is about 1.166 or 1.503 eV as shown in Tables I and III calculated within GGA and LDA, respectively. It is much bigger than the interlayer binding energy of graphite and $ZrTe_5$ [18] and Bi_4Br_4 [19]. In this point of view, the interlayer interaction in ZrSiO is weak covalent bonding rather than van der Waals interaction.

On the other hand, the band structure of single layer ZrSiO essentially has the same band topology as that in any plane perpendicular to k_z axis in 3D ZrSiO. The only difference is in the strength of particle-hole asymmetry. On considering these and the experimental technique of well controlled layer-by-layer growth of oxides [46], we think the single layer ZrSiO is readily synthesized. We perform full geometrical optimization of the free standing single layer ZrSiO. The cell parameters a and b have been relaxed to $a = b = 3.225$ Å. In the direction c, the atoms Zr move close to the Si layer by about 0.0251 Å, and the atoms O move close to the Si layer by about 0.004 Å. Such small relaxation can also be ascribed to its quasi-2D feature. The phonon spectrum of the fully relaxed structure is shown in Fig. 3. It has no imaginary frequency and indicates the dynamical stability of single layer ZrSiO.

The band structures shown in Figs. 2(b)–2(d) are for fully optimized 2D ZrSiO. As shown in Fig. 2(b), the two Dirac points on the paths Γ-X and Γ-M are nearly at the same energy level close to Fermi energy. When SOC is further considered, a global band gap around 0.01 eV is obtained as indicated by the total density of states (DOS) in Fig. 2(c) and the band structure in Fig. 2(d). The insets in Figs. 2(b) and 2(d) clearly show the gap opening by SOC along the node-line circle. We find that by slightly compressing the thickness of the slab or, equivalently, expanding the in-plane lattice constants would decrease the particle-hole asymmetry and change the size of band gap. For example, taking the experimental in-plane lattice constant and compressing the ZrSiO layer by 4% would lead to a global band gap about 30 meV.

Since it is central symmetric, the Z_2 number 1 is determined by counting the parity of all occupied states at four time reversal invariant momenta [25,26]. This confirms that the single slab of ZrSiO is a 2D TI. Its edge state along the a or b lattice vector is shown in Fig. 4, which is calculated using the Green's function method [3,5] based on the tight-binding Hamiltonian in the basis of Wannier functions of Zr d and Si p orbitals [35,36]. The edge states are characteristic Dirac-cone-like. We have also studied the decaying of edge state into the interior of 2D ZrSiO. As shown in Fig. 4(b), it decays quite slowly compared with the surface states of 3D TIs of Bi_2Se_3

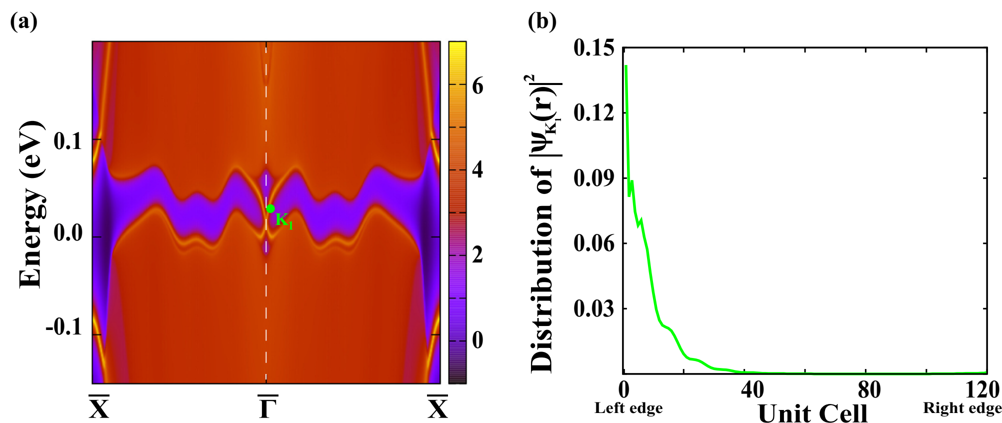

FIG. 4. (Color online) Edge state of single layer ZrSiO along a or b lattice vector. (a) The Dirac-cone-like edge state connects the bulk valence and conduction bands. (b) The wave function at the sampled k in (a) on the edge state shows its decay into bulk as a function of number of unit cell.

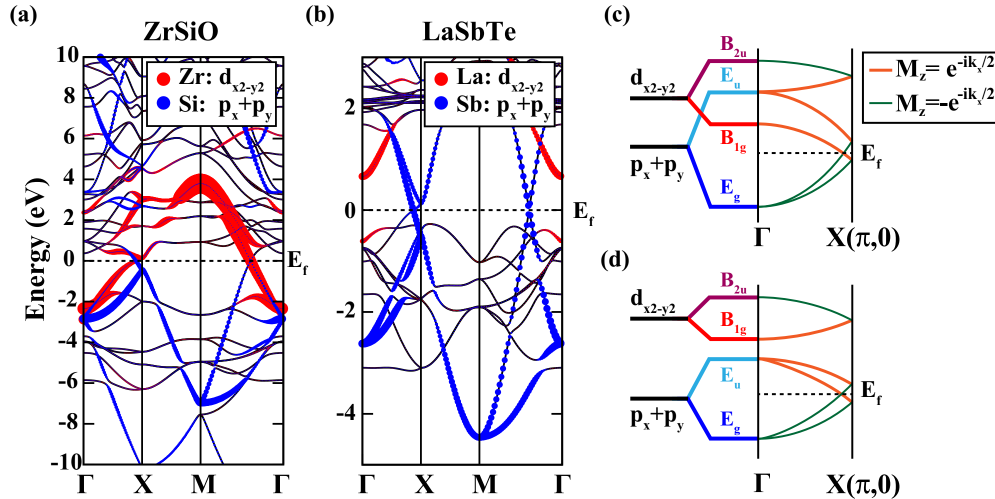

FIG. 5. (Color online) Band inversion mechanism in single layer ZrSiO. (a) The fatted band structure for Zr $d_{x^2-y^2}$ and Si $p_x + p_y$ orbitals. (b) The fatted band structure for La $5d_{x^2-y^2}$ and Sb $p_x + p_y$ orbitals. (c) and (d) are the band inversion mechanism with and without hybridization between $d_{x^2-y^2}$ and $p_x + p_y$ orbitals, corresponding to ZrSiO and LaSbTe, respectively.

or Bi_2Te_3. Therefore, a quite thick slab is needed, more than 80-unit-cells thick along a or b lattice, to get a gapless Dirac cone along its edge.

Band inversion mechanism. The crystal field splits five Zr d orbitals into $d_{x^2-y^2}$, d_{xy}, d_{z^2}, and $d_{yz} + d_{xz}$ manifolds and three Si p orbitals into p_z and $p_x + p_y$. The DOS plot and the fatted bands in Fig. 5(a) indicate that the bands involved in band inversion around the Fermi level are mainly composed of Zr $d_{x^2-y^2}$ and Si $p_x + p_y$ orbitals. In each unit cell, there are two nonequivalent Zr and Si atoms. The band inversion mechanism can be understood as follows. First, the degenerate atomic orbitals form the bonding and antibonding states, with the splitting determined by the effective hopping parameters of t_d and t_p. The bonding and antibonding states from $d_{x^2-y^2}$ orbitals constitute the B_{2u} (odd parity) and B_{1g} (even parity) representation of D_{4h}, the little group at Γ. Those from degenerate $p_x + p_y$ orbitals construct the 2D representation E_u and E_g of D_{4h}. It is noted that the $d_{xz} + d_{yz}$ of Zr atoms form the same 2D representation as $p_x + p_y$ orbitals and they are heavily hybridized. Secondly, the banding effect along Γ-X leads to band broadening and band inversion. As we note that both the glide mirror $\{M_z|(\frac{1}{2}, \frac{1}{2},0)\}$ (with ab plane

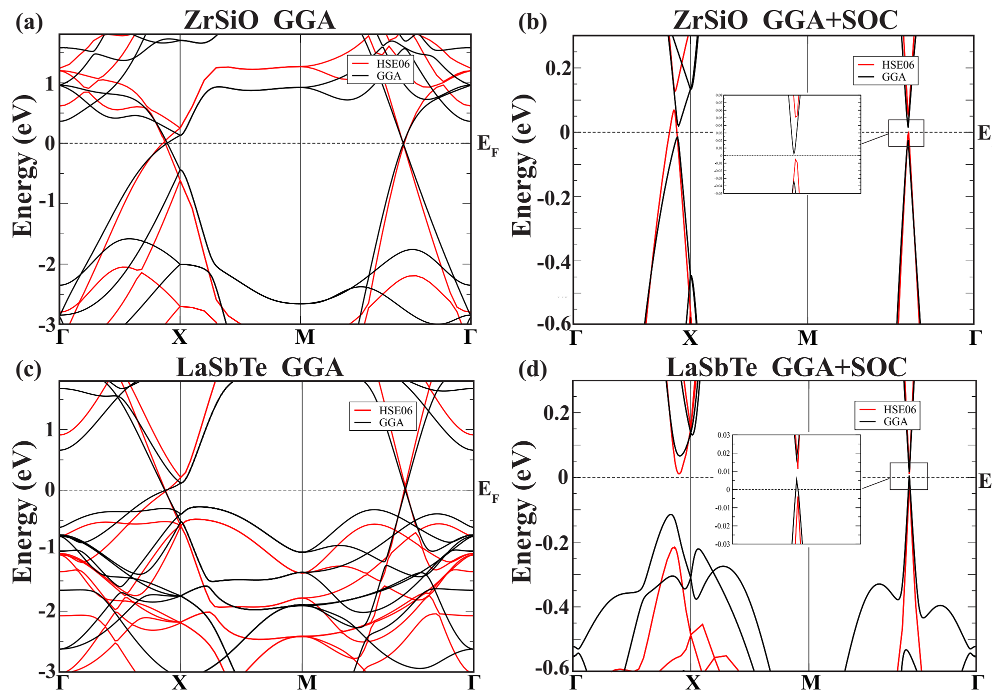

FIG. 6. (Color online) Band structures of (a) ZrSiO without SOC, (b) ZrSiO with SOC, (c) LaSbTe without SOC, and (d) LaSbTe with SOC, calculated within GGA (black lines) and HSE06 (red lines).

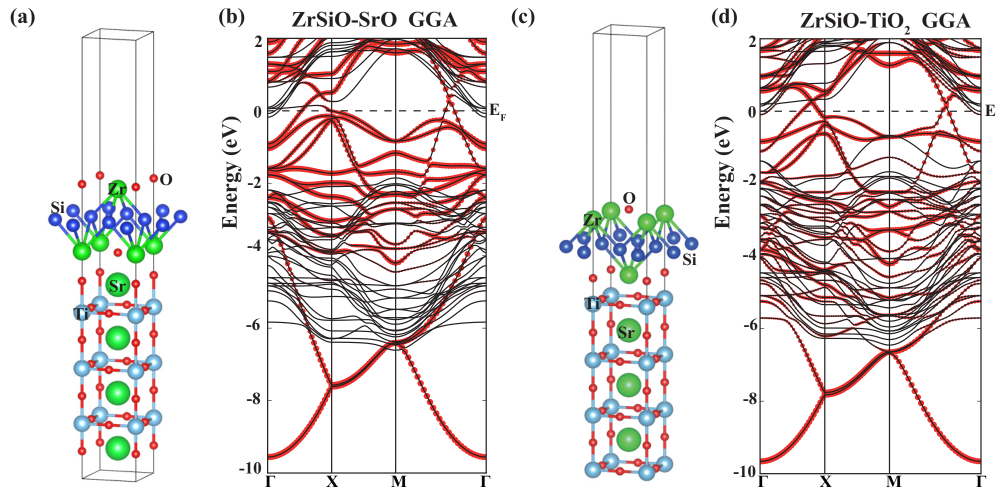

FIG. 7. (Color online) Geometrical structure and band structure of single layer ZrSiO on (a),(b) SrO terminated surface and (c),(d) TiO_2 terminated surface of $SrTiO_3$. The red circled lines are the fatted bands with the circle size proportional to the weight on single layer of ZrSiO.

as mirror plane) and the inversion symmetry P anticommute with the screw rotation $\{C_{2x}|(\frac{1}{2},0,0)\}$ at three TRIM points at the zone boundary X, Y, and M. As a consequence, similar to the situation in $ZrTe_5$ we can prove that all the states at those TRIM points at the zone boundary are doubly degenerate with opposite glide mirror eigenvalue and parity. This leads to a unique property that the Z_2 invariance here is determined by the order of states at Γ point, because all the contributions from the parity of the states at the zone boundary TRIM points always cancel each other. Since the states at X must be paired with glide mirror eigenstates with opposite eigenvalues $\pm e^{ik_x/2}$, as shown in Figs. 5(c) and 5(d), when the bands evolve from Γ to X, there are unavoidable band crossings for two typical order of states at Γ from two different such materials (ZrSiO and LaSbTe). As discussed in the previous section, these band crossings are protected by the glide mirror

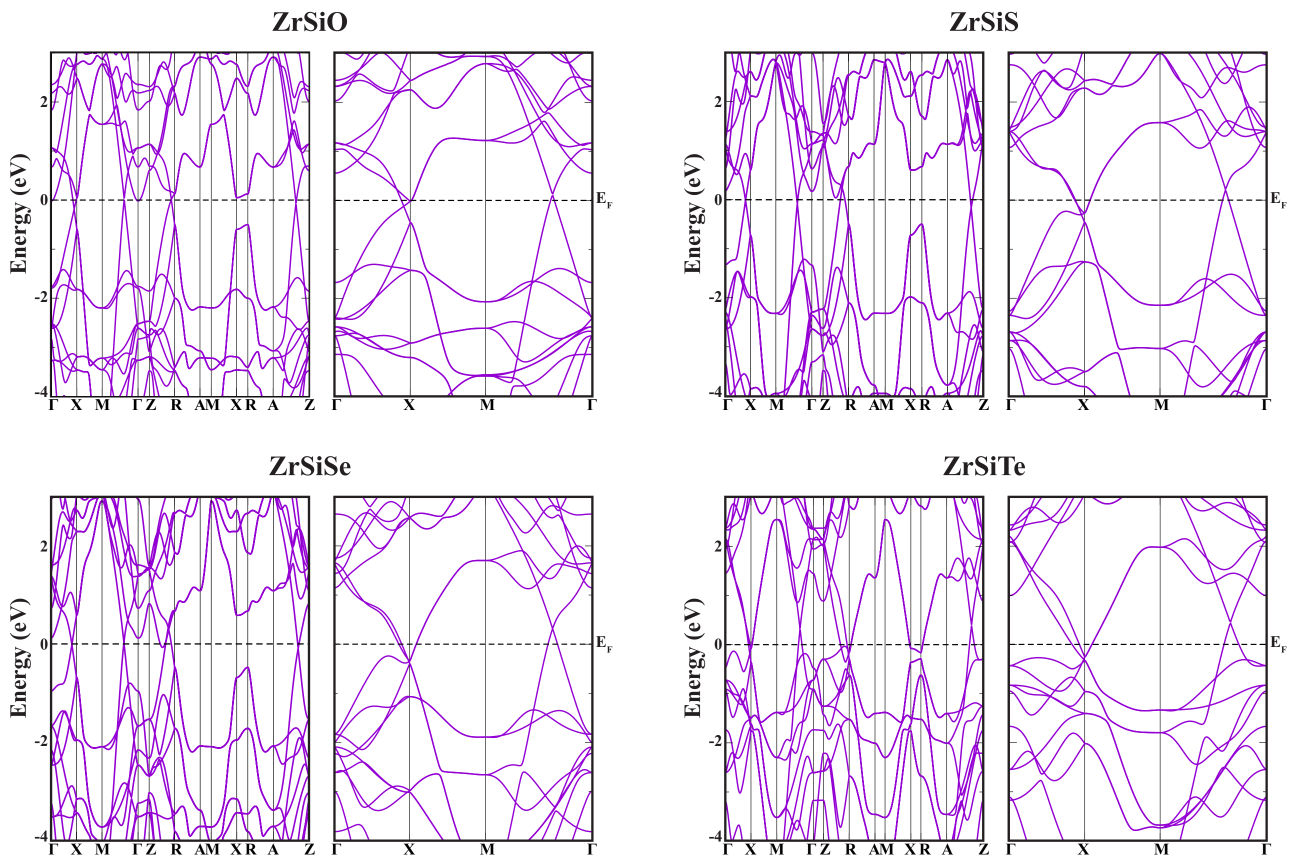

FIG. 8. (Color online) Band structure for (left) 3D and (right) 2D ZrSiM with M = O, S, Se, and Te. The experimental crystal structure of them are used.

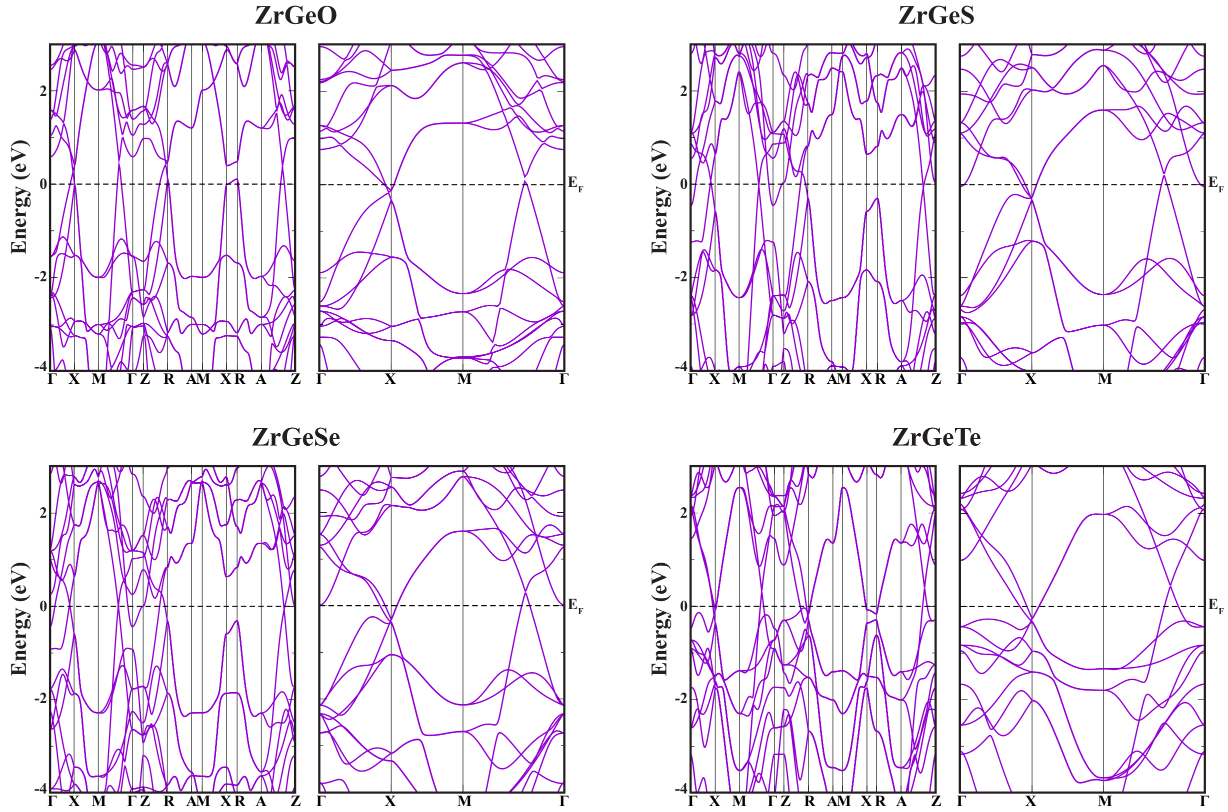

FIG. 9. (Color online) Band structure for (left) 3D and (right) 2D ZrGeM with M = O, S, Se, and Te. Except for the M = O case, the others are calculated with experimental structure. The experimental crystal structure of ZrSiO is used for ZrGeO.

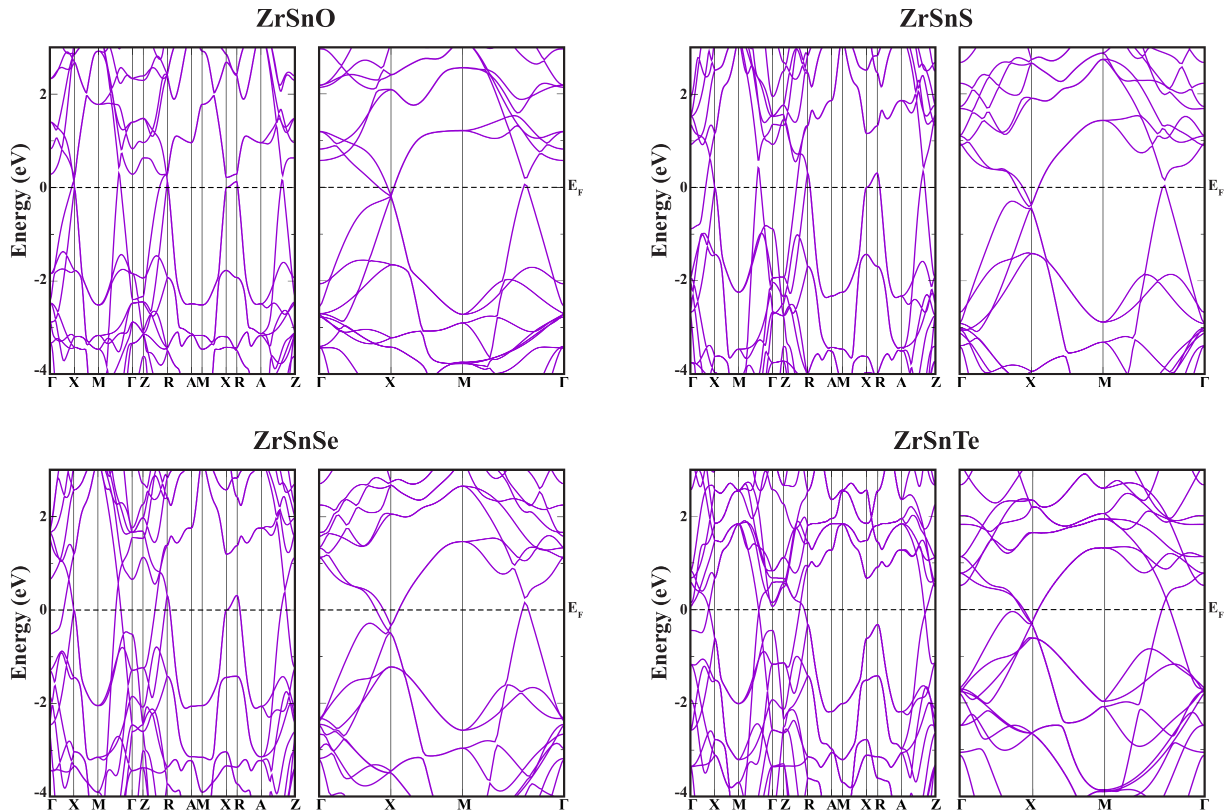

FIG. 10. (Color online) Band structure for (left) 3D and (right) 2D ZrSnM with M = O, S, Se, and Te. The experimental crystal structure of ZrSiO, ZrGeS, and ZrGeSe are used from ZrSnO, ZrSnS, and ZrSnSe, respectively.

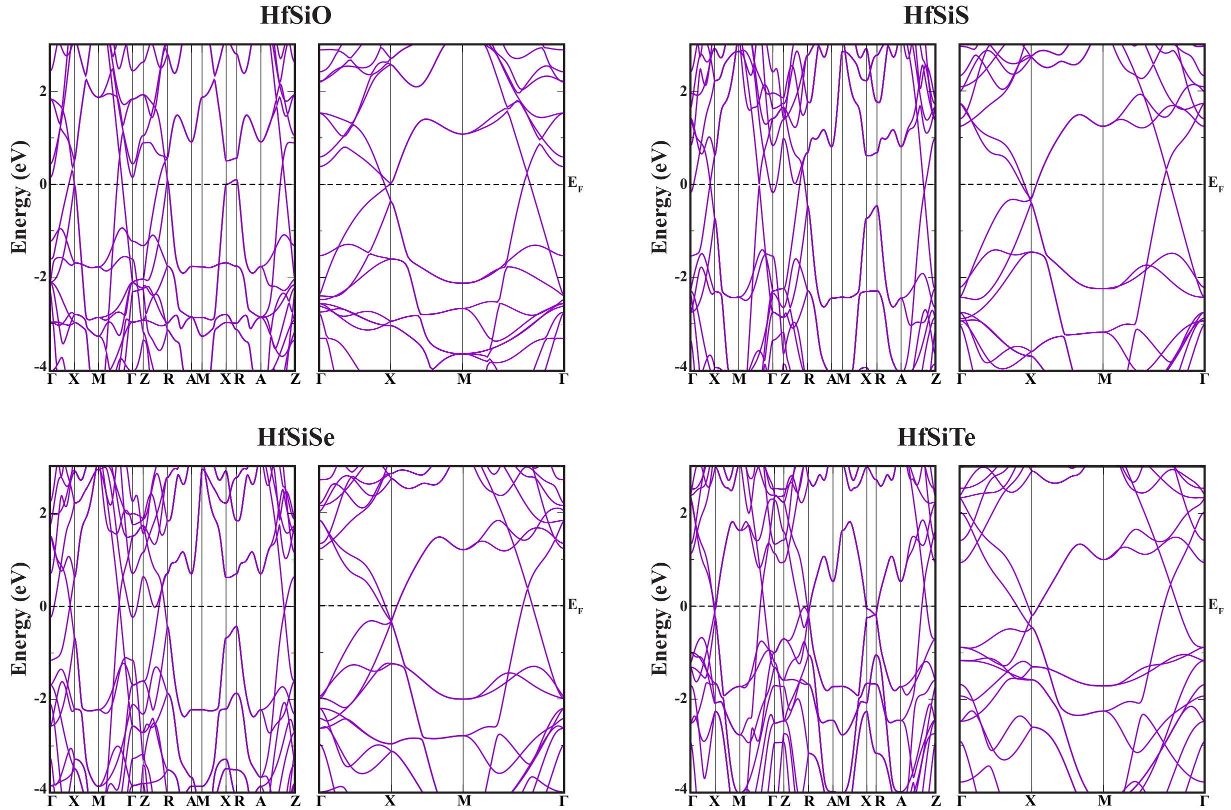

FIG. 11. (Color online) Band structure for (left) 3D and (right) 2D HfSiM with M = O, S, Se, and Te. The experimental crystal structure of HfSiS is used for HfSiO. For others the experimental crystal structure is used.

symmetry and form the node line inside of the mirror plane as shown in Fig. 2(b). With SOC included, the band gap will open in ZrSiO and its Z_2 invariance can be determined by the states at Γ point to be odd. The fitted band structure from the tight-binding model with basis of $d_{x^2-y^2}$ and $p_x + p_y$ orbitals can well reproduce the one from the first-principles calculation as shown in Fig. 5(c). The relative energy level of $d_{x^2-y^2}$, $p_x + p_y$, and Fermi level E_f determines the band topology. With the same number of electrons as ZrSiO, it is a trivial insulator if $d_{x^2-y^2}$ bands are fully occupied as shown in Fig. 5(c). However, if $d_{x^2-y^2}$ are higher than $p_x + p_y$ orbitals, the Fermi level will pass through the band crossing point and it becomes a 2D TI with SOC included. We find that the isostructural LaSbTe [38] with the same number of electrons exactly follows this picture and its band structure is shown in Fig. 5(b). The La 5d orbitals are full empty and have one less valence electron than Zr or Hf, while the Sb has one more valence electron than Si and other group IV elements. The single layer LaSbTe is a 2D TI with global band gap around 0.011 eV with SOC included. The band inversion and the band gap of ZrSiO and LaSbTe are further checked by HSE06 calculations in Fig. 6. We find that in both cases the band inversion is well kept. The particle-hole asymmetry in ZrSiO is modified a little and the global band gap is missing. For LaSbTe, the band gap is slightly increased to 0.015 eV.

Single layer ZrSiO on substrate SrTiO$_3$. In fact, the single layer material should be supported by substrate in experiment. To check the influence of substrate on the electronic structure of ZrSiO, we put a single layer of ZrSiO on commonly used substrate $SrTiO_3$. There are two types of top surface for $SrTiO_3$, namely, the SrO terminated surface and the TiO_2 terminated one, as shown in Figs. 7(a) and 7(c), respectively. Three unit cells of $SrTiO_3$ are taken as substrate. When ZrSiO is put on each surface, the cations are put on top of anions to minimize the total energy and the a, b lattice constants are expanded to

TABLE I. Binding energy of ZrHM (H = Si, Ge, Sn and M = O, S, Se, and Te) with GGA.

	Bulk energy (eV)	Single layer energy (eV)	Binding energy (eV)
ZrSiO	−46.1300	−44.9636	1.1664
ZrSiS	−43.3683	−42.9107	0.4576
ZrSiSe	−41.3001	−41.0870	0.2131
ZrSiTe	−37.5493	−38.4900	0.0593
ZrGeO(ZrSiO)	−43.8003	−42.6451	1.1552
ZrGeS	−41.3247	−40.7203	0.6044
ZrGeSe	−39.4017	−39.0765	0.3252
ZrGeTe	−37.2003	−37.0285	0.1718
ZrSnO(ZrSiO)	−37.1185	−36.0409	1.0776
ZrSnS(ZrGeS)	−36.2699	−35.7437	0.5262
ZrSnSe(ZrGeSe)	−35.1396	−34.8805	0.2591
ZrSnTe	−35.3951	−34.7090	0.6861

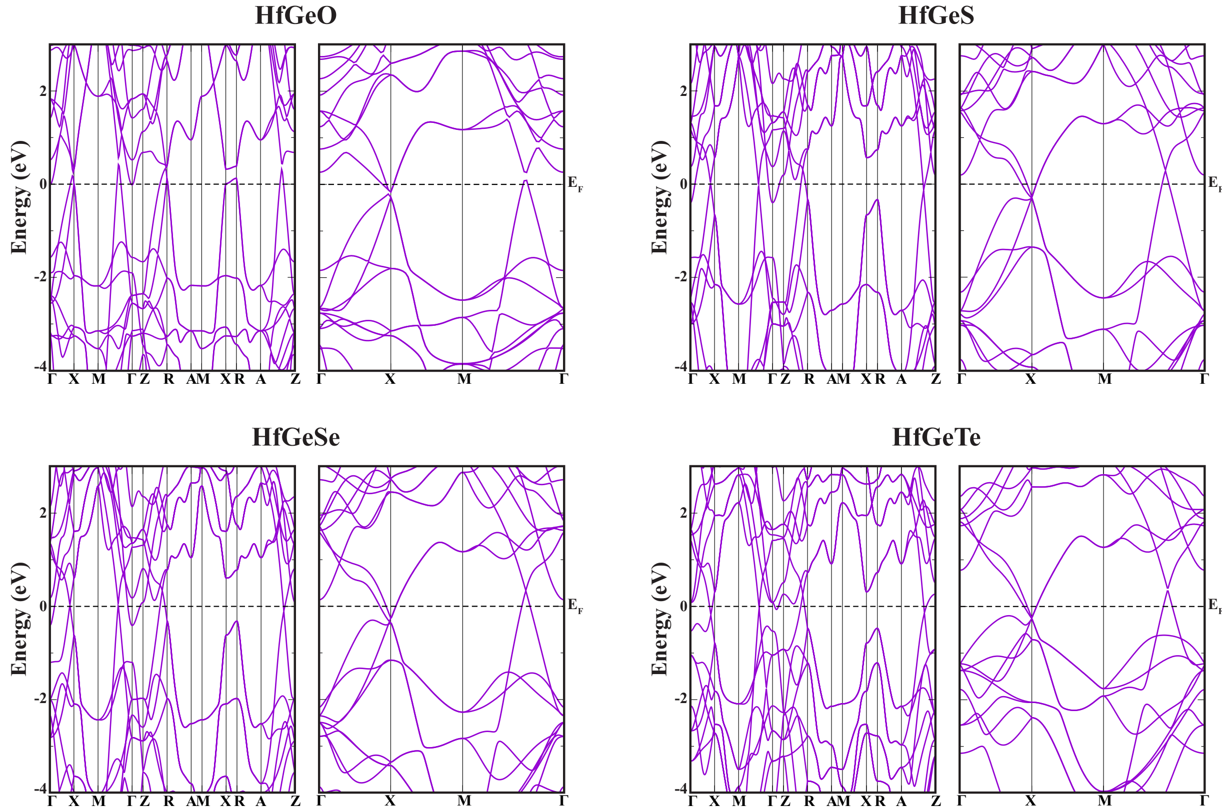

FIG. 12. (Color online) Band structure for (left) 3D and (right) 2D HfGeM with $M = O$, S, Se, and Te. The experimental crystal structure of HfSiS is used for HfGeO. For others the experimental crystal structure is used.

fit the $SrTiO_3$ substrate. The initial distance of them is about half of the cell parameter of $SrTiO_3$. A vacuum about 13 Å thick is also used here. The three-layer atoms of $SrTiO_3$ at the interface and all atoms of single layer ZrSiO are fully relaxed. The geometrical structure has nearly no change. The fatted bands with weight on single layer of ZrSiO are shown in Figs. 7(b) and 7(d). We find that most features of free standing ZrSiO are well kept, especially the band crossings around the Fermi level are well reproduced inside of the band gap

TABLE II. Binding energy of HfHM ($H =$ Si, Ge, Sn and $M =$ O, S, Se, and Te) with GGA.

	Bulk energy (eV)	Single layer energy (eV)	Binding energy (eV)
HfSiO(HfSiS)	−48.0666	−46.7249	1.3417
HfSiS	−45.8371	−45.4245	0.4126
HfSiSe	−43.6437	−43.4343	0.2095
HfSiTe	−41.2764	−41.2495	0.0269
HfGeO(HfSiS)	−45.6977	−44.3726	1.3251
HfGeS	−43.6926	−43.0004	0.6922
HfGeSe	−41.6818	−41.2514	0.4304
HfGeTe	−39.3686	−39.1276	0.2410
HfSnO(HfSiS)	−39.0500	−37.8001	1.2499
HfSnS(HfSiS)	−36.9242	−36.6204	0.3038
HfSnSe(HfGeSe)	−37.2744	−36.9109	0.3635
HfSnTe(HfGeTe)	−35.7217	−35.5274	0.1943

of $SrTiO_3$ substrate. On considering the underestimation of $SrTiO_3$ band gap by about 2.0 eV within GGA, we believe that $SrTiO_3$ is quite suitable for supporting ZrSiO.

The WHM family. We have further calculated the other isostructural compounds WHM with $W =$ Zr, Hf, $H =$ Si, Ge, Sn, and $M =$ O, S, Se and Te. The band structures for both the 3D and single layer 2D WHM have been shown in Figs. 8, 9, 10, 11, 12, and 13. All of these bands show the similar band structure around the Fermi level. The difference is the strength of particle-hole asymmetry, which make it possible for most of them to be semimetals with overlapped electron-hole pockets. As we have discussed above, the expansion in a, b lattice constant and compression of the slab thickness can be helpful in decreasing the asymmetry and thus leads to the global band gap. From these figures, we find the particle-hole asymmetry increases as M changes from O to Te. At the same time, the binding energy between layers with GGA in Tables I and II

TABLE III. Binding energy of ZrSiM ($M =$ O, S, Se, and Te) with LDA.

	Bulk energy (eV)	Single layer energy (eV)	Binding energy (eV)
ZrSiO	−50.0572	−48.5542	1.5030
ZrSiS	−47.9620	−46.9407	1.0213
ZrSiSe	−45.9505	−45.2032	0.7473
ZrSiTe	−43.0325	−42.6953	0.3372

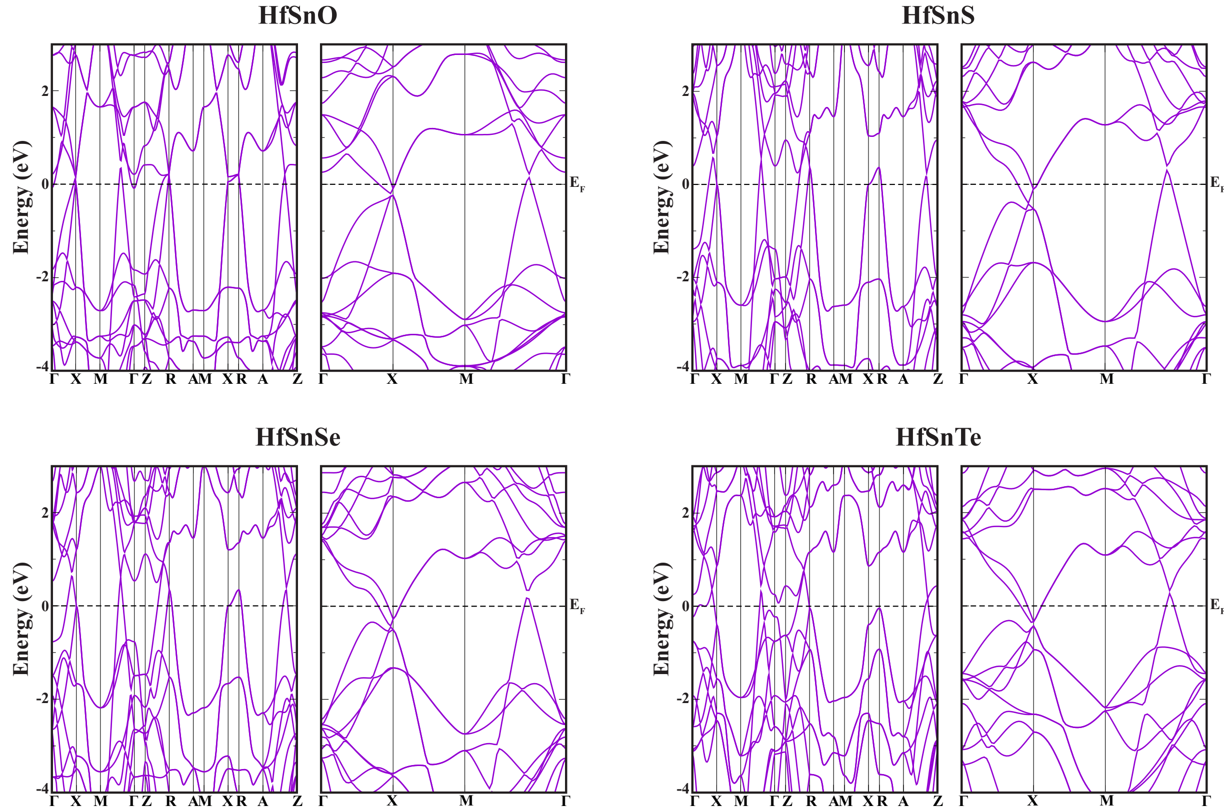

FIG. 13. (Color online) Band structure for (left) 3D and (right) 2D HfSnM with M = O, S, Se, and Te. The experimental crystal structure of HfSiS is used for HfSnO and HfSnS. That of HfGeSe and HfGeTe is used for HfSnSe and HfSnTe, respectively.

decreases when M changes from O to Te. It is also validated by the example of ZrSiM with LDA in Table III. Therefore, the further detailed works on the WHM family are necessary and left for successive papers.

IV. CONCLUSIONS

Based on the first-principles calculations, we have predicted that 3D ZrSiO is a weak TI and its single layer ZrSiO is an oxide 2D TI with band gap around 30 meV. The other members in this family noted as WHM with W = Zr, Hf, H = Si, Ge, Sn, and M = O, S, Se, and Te have the similar band structure and are most probably 2D TIs. The isoelectronic compound LaSbTe has been shown to share the similar band structure and share the same underlying physics in band inversion.

ACKNOWLEDGMENTS

We acknowledge support from National Natural Science Foundation of China (Grants No. 11274359 and No. 11422428), the National 973 program of China (Grants No. 2011CBA00108 and No. 2013CB921700), and the "Strategic Priority Research Program (B)" of the Chinese Academy of Sciences (Grant No. XDB07020100). Part of the calculations were performed on TianHe-1(A), the National Supercomputer Center in Tianjin, China.

[1] M. Z. Hasan and C. L. Kane, Colloquium: Topological insulators, Rev. Mod. Phys. **82**, 3045 (2010).

[2] X.-L. Qi and S.-C. Zhang, Topological insulators and superconductors, Rev. Mod. Phys. **83**, 1057 (2011).

[3] H. Weng, R. Yu, X. Hu, X. Dai, and Z. Fang, Quantum anomalous Hall effect and related topological electronic states, Adv. Phys. **64**, 227 (2015).

[4] H. Weng, A. Ranjbar, Y. Liang, Z. Song, M. Khazaei, S. Yunoki, M. Arai, Y. Kawazoe, Z. Fang, and X. Dai, Large-gap two-dimensional topological insulator in oxygen functionalized mxene, Phys. Rev. B **92**, 075436 (2015).

[5] H. Weng, X. Dai, and Z. Fang, Exploration and prediction of topological electronic materials based on first-principles calculations, MRS Bull. **39**, 849 (2014).

[6] L. Fu and C. L. Kane, Superconducting Proximity Effect and Majorana Fermions at the Surface of a Topological Insulator, Phys. Rev. Lett. **100**, 096407 (2008).

[7] Y. Ando, Topological insulator materials, J. Phys. Soc. Jpn. **82**, 102001 (2013).

[8] B. A. Bernevig, T. L. Hughes, and S.-C. Zhang, Quantum spin Hall effect and topological phase transition in HgTe quantum wells, Science **314**, 1757 (2006).

[9] M. König, S. Wiedmann, C. Brüne, A. Roth, H. Buhmann, L. W. Molenkamp, X.-L. Qi, and S.-C. Zhang, Quantum spin Hall insulator state in HgTe quantum wells, Science **318**, 766 (2007).

[10] I. Knez, R.-R. Du, and G. Sullivan, Evidence for Helical Edge Modes in Inverted InAs/GaSb Quantum Wells, Phys. Rev. Lett. **107**, 136603 (2011).

[11] C.-C. Liu, W. Feng, and Y. Yao, Quantum Spin Hall Effect in Silicene and Two-Dimensional Germanium, Phys. Rev. Lett. **107**, 076802 (2011).

[12] Y. Xu, B. Yan, H.-J. Zhang, J. Wang, G. Xu, P. Tang, W. Duan, and S.-C. Zhang, Large-gap Quantum Spin Hall Insulators in Tin Films, Phys. Rev. Lett. **111**, 136804 (2013).

[13] C. Si, J. Liu, Y. Xu, J. Wu, B.-L. Gu, and W. Duan, Functionalized germanene as a prototype of large-gap two-dimensional topological insulators, Phys. Rev. B **89**, 115429 (2014).

[14] Z. Song, C.-C. Liu, J. Yang, J. Han, M. Ye, B. Fu, Y. Yang, Q. Niu, J. Lu, and Y. Yao, Quantum spin Hall insulators and quantum valley Hall insulators of BiX/SbX (X=H, F, Cl and Br) monolayers with a record bulk band gap, NPG Asia Mater. **6**, e147 (2014).

[15] Y. Ma, Y. Dai, L. Kou, T. Frauenheim, and T. Heine, Robust two-dimensional topological insulators in methyl-functionalized bismuth, antimony, and lead bilayer films, Nano Lett. **15**, 1083 (2015).

[16] Y. Ma, X. Li, L. Kou, B. Yan, C. Niu, Y. Dai, and T. Heine, Two-dimensional inversion-asymmetric topological insulators in functionalized iii-bi bilayers, Phys. Rev. B **91**, 235306 (2015).

[17] W. Luo and H. Xiang, Room temperature quantum spin Hall insulators with a buckled square lattice, Nano Lett. **15**, 3230 (2015).

[18] H. Weng, X. Dai, and Z. Fang, Transition-metal Pentatelluride $ZrTe_5$ and $HfTe_5$: A Paradigm for Large-gap Quantum Spin Hall Insulators, Phys. Rev. X **4**, 011002 (2014).

[19] J.-J. Zhou, W. Feng, C.-C. Liu, S. Guan, and Y. Yao, Large-gap quantum spin Hall insulator in single layer bismuth monobromide Bi_4 Br_4, Nano Lett. **14**, 4767 (2014).

[20] X. Qian, J. Liu, L. Fu, and J. Li, Quantum spin Hall effect in two-dimensional transition metal dichalcogenides, Science **346**, 1344 (2014).

[21] S. M. Nie, Z. Song, H. Weng, and Z. Fang, Quantum spin Hall effect in two-dimensional transition-metal dichalcogenide haeckelites, Phys. Rev. B **91**, 235434 (2015).

[22] Z. Song, S. M. Nie, H. Weng, and Z. Fang, Quantum spin Hall state on square-like lattice, arXiv:1508.05220.

[23] Y. Sun, C. Felser, and B. Yan, Graphene-like Dirac states and quantum spin Hall insulators in the square-octagonal MX_2 (M = Mo, W; X = S, Se, Te) isomers, Phys. Rev. B **92**, 165421 (2015).

[24] Y. Ma, L. Kou, Y. Dai, and T. Heine, Quantum spin Hall effect and topological phase transition in two-dimensional square transition metal dichalcogenides, Phys. Rev. B **92**, 085427 (2015).

[25] L. Fu, C. L. Kane, and E. J. Mele, Topological Insulators in Three Dimensions, Phys. Rev. Lett. **98**, 106803 (2007).

[26] J. E. Moore and L. Balents, Topological invariants of time-reversal-invariant band structures, Phys. Rev. B **75**, 121306 (2007).

[27] R. Roy, Z_2 classification of quantum spin Hall systems: An approach using time-reversal invariance, Phys. Rev. B **79**, 195321 (2009).

[28] G. Kresse and J. Furthmüller, Efficiency of ab-initio total energy calculations for metals and semiconductors using a plane-wave basis set, Comput. Mater. Sci. **6**, 15 (1996).

[29] G. Kresse and J. Furthmüller, Efficient iterative schemes for ab initio total-energy calculations using a plane-wave basis set, Phys. Rev. B **54**, 11169 (1996).

[30] J. Perdew, K. Burke, and M. Ernzerhof, Generalized Gradient Approximation Made Simple, Phys. Rev. Lett. **77**, 3865 (1996).

[31] J. Heyd, G. E. Scuseria, and M. Ernzerhof, Hybrid functionals based on a screened Coulomb potential, J. Chem. Phys. **118**, 8207 (2003).

[32] J. Heyd, G. E. Scuseria, and M. Ernzerhof, Erratum: "Hybrid functionals based on a screened Coulomb potential" [J. Chem. Phys. **118**, 8207 (2003)], J. Chem. Phys. **124**, 219906 (2006).

[33] N. Marzari and D. Vanderbilt, Maximally localized generalized Wannier functions for composite energy bands, Phys. Rev. B **56**, 12847 (1997).

[34] I. Souza, N. Marzari, and D. Vanderbilt, Maximally localized Wannier functions for entangled energy bands, Phys. Rev. B **65**, 035109 (2001).

[35] http://www.openmx-square.org.

[36] H. Weng, T. Ozaki, and K. Terakura, Revisiting magnetic coupling in transition-metal-benzene complexes with maximally localized Wannier functions, Phys. Rev. B **79**, 235118 (2009).

[37] H. Onken, K. Vierheilig, and H. Hahn, Über silicid- und germanidchalkogenide des zirkons und hafniums, Z. Anorg. Allg. Chem. **333**, 267 (1964).

[38] C. Wang and T. Hughbanks, Main group element size and substitution effects on the structural dimensionality of zirconium tellurides of the ZrSiS type, Inorg. Chem. **34**, 5524 (1995).

[39] W. Bensch, O. Helmer, M. Muhler, H. Ebert, and M. Knecht, Experimental and theoretical band structure of the layer compound ZrSiTe, J. Phys. Chem. **99**, 3326 (1995).

[40] G. Ryu, S. W. Kim, H. Mizoguchi, S. Matsuishi, and H. Hosono, Superconductivity in a pbfcl-type pnictide: Nbsias, Europhys. Lett. **99**, 27002 (2012).

[41] X. C. Wang, Q. Q. Liu, Y. X. Lv, W. B. Gao, L. X. Yang, R. C. Yu, F. Y. Li, and C. Q. Jin, The superconductivity at 18 K in LiFeAs system, Solid State Commun. **148**, 538 (2008).

[42] H. Weng, C. Fang, Z. Fang, B. A. Bernevig, and X. Dai, Weyl Semimetal Phase in Noncentrosymmetric Transition-metal Monophosphides, Phys. Rev. X **5**, 011029 (2015).

[43] H. Weng, Y. Liang, Q. Xu, R. Yu, Z. Fang, X. Dai, and Y. Kawazoe, Topological node-line semimetal in three-dimensional graphene networks, Phys. Rev. B **92**, 045108 (2015).

[44] R. Yu, H. Weng, Z. Fang, X. Dai, and X. Hu, Topological Node-line Semimetal and Dirac Semimetal State in Antiperovskite Cu_3 PdN, Phys. Rev. Lett. **115**, 036807 (2015).

[45] Y. Kim, B. J. Wieder, C. L. Kane, and A. M. Rappe, Dirac Line Nodes in Inversion-symmetric Crystals, Phys. Rev. Lett. **115**, 036806 (2015).

[46] H. Y. Hwang, Y. Iwasa, M. Kawasaki, B. Keimer, N. Nagaosa, and Y. Tokura, Emergent phenomena at oxide interfaces, Nat. Mater. **11**, 103 (2012).